Journal of Applied Physics ARTICLE scitation.org/journal/jap

Effects of grain boundary structures on primary radiation damage and radiation-induced segregation in austenitic stainless steel

Cite as: J. Appl. Phys. **128**, 105304 (2020); doi: 10.1063/5.0016404
Submitted: 4 June 2020 · Accepted: 30 August 2020 ·
Published Online: 14 September 2020

Jing Gao,[1] Feida Chen,[1,2,a)] Xiaobin Tang,[1,2,a)] Guojia Ge,[1] Jiwei Lin,[1] and Shangkun Shen[1]

AFFILIATIONS

[1]Department of Nuclear Science and Technology, Nanjing University of Aeronautics and Astronautics, Nanjing 211106, China
[2]Key Laboratory of Nuclear Technology Application and Radiation Protection in Astronautics, Nanjing University of Aeronautics and Astronautics, Ministry of Industry and Information Technology, Nanjing 211106, China

[a)]**Authors to whom correspondence should be addressed:** fdchen@nuaa.edu.cn and tangxiaobin@nuaa.edu.cn

ABSTRACT

Grain boundary (GB) engineering is crucial in the austenitic stainless steel (ASS) design for nuclear energy applications. In this work, the influence of different GB structures on radiation defect recombination and radiation-induced segregation (RIS) at different temperatures were investigated using molecular dynamics simulation. Four typical GBs in ASSs were selected as model structures. Results showed that GBs remained stable at various temperatures and they all exhibited better self-healing performance than single crystals in terms of radiation defects. However, except Σ3(112) GB, other three GBs cannot inhibit the radiation induced segregation, while promoting the radiation defect recombination. Calculation results showed that the higher Σ value of GBs can lead to a greater lattice mismatch near GBs, which not only results in stronger sink strength for radiation induced defects, but also provides more sites for solute atoms and causes greater segregations eventually. Owing to the intrinsic low Σ and large inclination angle characteristic, Σ3(112) GB achieves an excellent balance between the defect-absorption and RIS. This phenomenon provides a feasible route for the future GB design in ultra-high radiation tolerant materials.

I. INTRODUCTION

Austenitic stainless steels (ASSs) with high resistance to corrosion and high-temperature creep strength are widely used in current pressurized water reactors (PWRs) as structural materials for internal components.[1–3] With the development of the next-generation advanced nuclear reactor technology, materials need to withstand higher service temperatures and radiation doses. This phenomenon poses great challenges to the radiation resistance of ASSs. Grain boundaries (GBs) play a crucial role in the radiation resistance,[4] corrosion,[5,6] and mechanical properties[7,8] of metallic materials. Massive experiments and atomistic modeling have verified the effect of GBs on cascade-induced point defect absorption in fcc and bcc metals.[9–13] Although previous studies reported that the presence of GBs would influence defect production, a few works have focused on the whole effects caused by different GB types, including the radiation induced defect absorption and radiation induced segregation in the complex fcc structure ASS systems.

As it has been shown, mechanical property degradation under neutron-radiation mainly depends on the production and evolution of radiation-induced defects;[14,15] in this regard, a few research studies have been conducted to investigate the microstructure evolution of ASSs under severe irradiation conditions.[16–18] Samaras *et al.*[19] performed molecular dynamics (MD) simulation and deduced that collision cascades interacting with GBs modify the produced defects significantly, which promoted the production of stacking-fault tetrahedral. Bai *et al.*[11] found by using long timescale simulation techniques that the interstitials captured at the GB re-emit to recombine with vacancies near the GB, thus resulting in the recovery of damage. Extensive experimental efforts have been devoted to explore the effect of GBs on radiation responses.[20–22] Singh and Foreman[20] confirmed that the radiation-induced damage decreased with grain size due to the defect absorption at GBs in ASSs.

Materials used in extreme environments also undergo non-equilibrium segregation, which ultimately leads to changes in the local microstructure and microchemistry.[23,24] Interstitials and vacancies generally interact quite differently with solute species in alloy. Meanwhile, the diffusive fluxes of interstitials or vacancies toward point-defect sinks often produce concomitant preferential fluxes of atoms. Radiation-induced segregation (RIS) is the result of long-range, radiation-induced, solute redistribution at point-defect sinks. RIS could cause Ni enrichment and Cr depletion in the vicinity of GBs in austenitic alloys, while whether Fe will enrich or deplete depends on bulk alloy compositions. The depletion of Cr may cause GBs to be susceptible to corrosion and induce irradiation-assisted stress corrosion cracking.[25] Numerous studies have proved that RIS is related to the GB structures. Kai and co-workers[26,27] found the local minima of segregation at Σ3 GB and noted a universal trend of low Cr segregation with the decreasing coincident site lattice (CSL) Σ value, where Σ represented the degree of geometrical coincidence at the GB. Watanabe *et al.*[28] found that Σ3, Σ9, and low-tilt-angle GBs reduced Cr depletion, whereas more random and high-angle tilt GBs did not suppress RIS.

In this work, the effects of GB structure and temperature on the annihilation of defects and segregation near the GBs were studied by MD simulation. Four common Fe–Cr–Ni random bi-crystals in ASSs were selected. The evolution of defects and their interaction with GBs at various temperatures were discussed.

II. MODELS AND METHODS

Molecular statics (MS) and MD simulations were carried out in the large-scale atomic/molecular massively parallel simulator code LAMMPS.[29] All simulation boxes and GB structures were constructed by using the open source program Atomsk.[30] Ovito[31] was used to visualize and analyze the atomistic configurations and point defects. Periodic boundary conditions were applied along all directions during all simulations.

For the equivalent austenite stainless material system, fcc elementary cells with the lattice constant $a_0 = 3.521\,96$ Å[32] were established. The fcc sites of the supercell were randomly filled with Fe, Ni, and Cr atoms and satisfied two conditions:[33] (1) the alloy compositions (Fe, Ni, and Cr) exhibit a homogeneous distribution and (2) the alloy is composed of (in atomic percentage) 67.2% Fe, 18.8% Cr, and 14.0% Ni, which is similar to AISI-316L alloys.[34]

The configurations of GBs are shown in Fig. 1. The interaction between the modeled alloys was described using an embedded atom model (EAM) potential developed by Bonny *et al.*[35] This potential was developed to study the production and evolution of radiation defects, particularly, point defects. The system sizes of various GB structures varied from 218 592 atoms ($116.22 \times 179.31 \times 114.56$ Å^3) to 232 960 atoms ($125.71 \times 179.58 \times 112.70$ Å^3) depending on the repeat unit of a GB structure.

In this work, we concentrated on the properties of four common GBs in ASSs: Σ3(111) coherent twin boundary, Σ3(112) symmetric incoherent twin boundary, and Σ9(114) and Σ13(510) symmetric GBs. The GB structure was constructed by rotating two grains at the same specific angle in opposite directions.[36] The upper and lower crystals in the simulation had different crystal orientations relative to the simulation box. For both crystals, the tilt axis was aligned along the Z direction, and the GB planes were normal to the Y direction. The details of the tilt angles, crystallographic orientation, and energy of the four investigated GBs are summarized in Table I. The crystal size was sufficiently large to avoid the interaction of cascade and sub-cascade with their periodic images and to ensure that the defects were maintained within the simulation box. The GBs were equilibrated using the conjugate gradient method by the MS technique to reach the entire lowest energy configuration. GB energy (E_{GB}) was calculated based on Ref. 36,

$$E_{GB} = \frac{E_{tot} - N \cdot E_{coh}}{2A}, \tag{1}$$

where E_{tot} is the total (potential) energy of the system, E_{coh} is the cohesive energy of an atom, A is the area of the GB, and N is the number of atoms.

The system was initially relaxed at the NPT ensemble with number of atoms (N), pressure (P) and temperature (T) conserved for 40 ps until each system reached a stable state. Simulations were carried out at 300 K, 600 K, 900 K, and 1000 K to determine the effect of temperature. At each temperature, 10 cascade simulations were performed to reduce the statistical error in the result. An atom was chosen as the primary knock-on atom (PKA) with 4 keV of kinetic energy, which was set as 20 Å from the GB at the start. The damage energy and PKA distance from the GB, being similar to what is reported by Xu *et al.*,[33] were selected such that the cascade interacted with the GB mostly and the center of cascade position was located on the GB plane (prefect overlap) as shown in Fig. S1 of the supplementary material. The velocity was perpendicular to the GB. During a collision cascade, the time step was 10^{-5} ps for the first 1 ps and then was increased to a larger time step of 10^{-4} ps for 2 ps. In the progress, the Nose–Hoover heat bath method was applied to maintain a constant temperature of the system, such that the excess kinetic energy introduced by PKA can be dissipated as in experimental situations.[37–39] Atoms within the "active region" were limited to move adiabatically through the NVE ensemble (constant number of atoms, volume, and energy).[40] Eventually, the time step was increased to 0.002 ps for about 60 ps to further anneal the system. Equivalent simulations in the single–crystal system were performed for comparison. The simulation methods and the orientation and energy of the PKA used in the single-crystal were consistent with those of the GB system. Cascade overlaps were carried out to study the influence of GBs under long-term irradiation. In continuous bombardment simulation, a cascade was started by imparting a PKA with 4 keV at 20 Å from the GB according to the method described above. The stabilization for defects was achieved by relaxation for sufficient time. In order to quickly release the system stress after the cascade, the crystal containing the defects created by the above cascade was quenched to 0.1 K,[41,42] following which it was re-equilibrated at the required temperature after 20 ps and then, second cascade (the overlap event) was initiated. Up to 10 cascades were set in the simulation cell. After cascade simulation, the point defects and defect cluster distributions were analyzed using common neighbor analysis (CNA) and Wigner–Seize cell.[43,44] In the present work, only defects remaining in the bulk region as defined in Fig. S3 of the

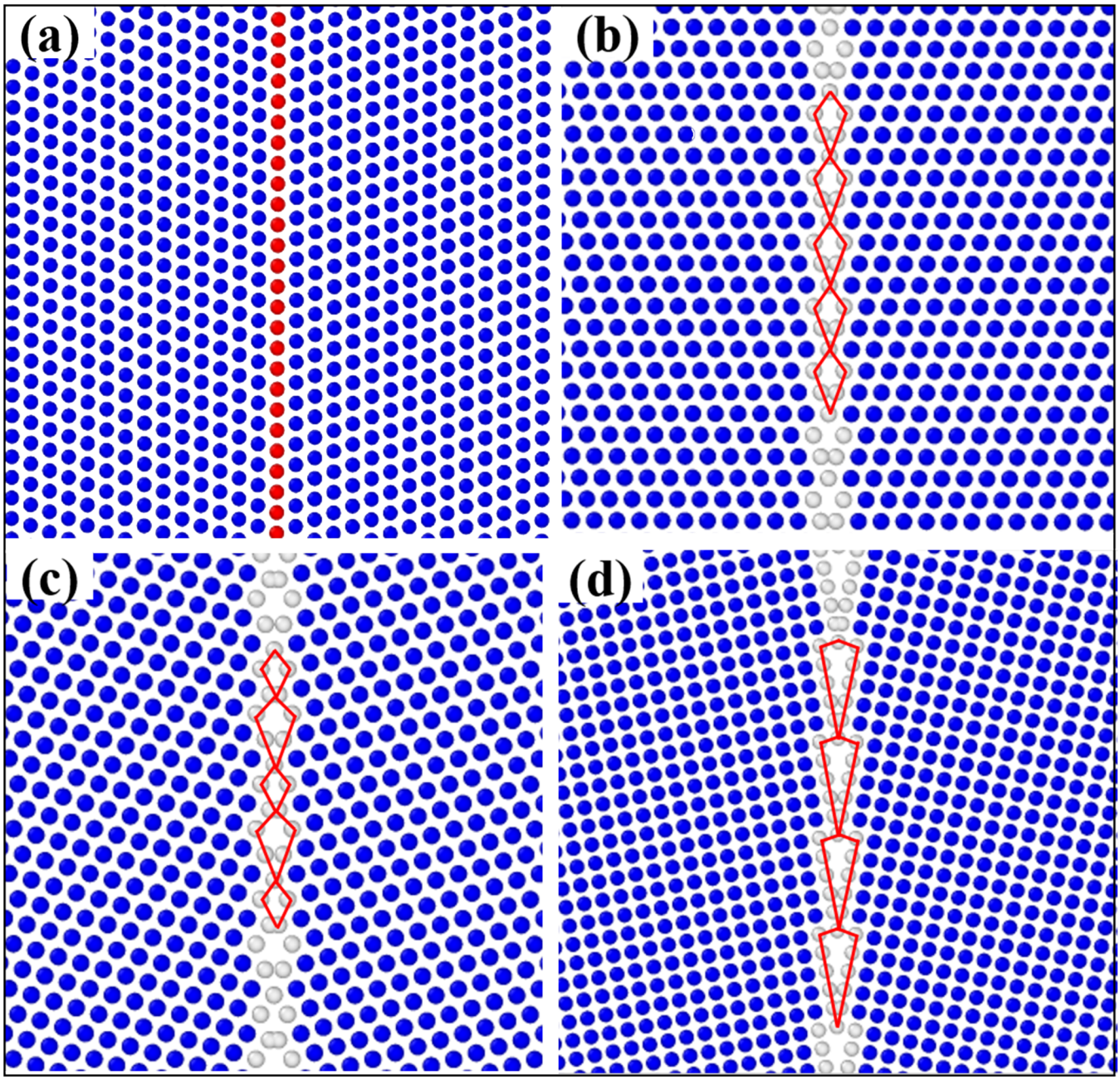

FIG. 1. Configurations of four different GBs: (a) Σ3(111) GB, (b) Σ3(112) GB, (c) Σ9(114) GB, and (d) Σ13(510) GB. The red lines outline the "kite" structures in different GBs, and Σ3(111) has no structural unit.

supplementary material were counted as the surviving ones to avoid considering rearrangements in the GB as defects.

The MS technique was used to calculate the formation energy of a vacancy and an interstitial in and around GBs for different GB configurations. The defect formation energy for a particular site α can be calculated using Eq. (2),

$$E_f^{\alpha} = E_{GB}^{\alpha} - E_{GB} \pm E_{coh}, \tag{2}$$

where E_{coh} is the cohesive energy per atom of a perfect fcc lattice of FeCrNi, and E_{GB}^{α} and E_{GB} are the total energies of the simulation cell with and without the defect, respectively. The only difference

TABLE I. Tilt angles, crystallographic orientation, and energy of four investigated grain boundaries (GBs).

GB type	Tilt angle (°)	Upper grain			Lower grain			E_{GB} (J/m^2)
		X	Y	Z	X	Y	Z	
Σ3(111)	70.53	[$\bar{1}$12]	[1$\bar{1}$1]	[110]	[$\bar{1}$1$\bar{2}$]	[$\bar{1}$11]	[110]	0.005
Σ3(112)	109.47	[$\bar{1}$11]	[1$\bar{1}$2]	[110]	[$\bar{1}$1$\bar{1}$]	[$\bar{1}$12]	[110]	1.528
Σ9(114)	38.94	[$\bar{2}$2$\bar{1}$]	[$\bar{1}$14]	[110]	[$\bar{2}$21]	[1$\bar{1}$4]	[110]	1.997
Σ13(510)	22.62	[05$\bar{1}$]	[015]	[100]	[051]	[0$\bar{1}$5]	[100]	2.016

in the calculation of formation energy of defect atoms is to add or subtract the cohesive energy from the system. The sites were selected from 40 Å from one side of the GB to 40 Å on the other side with a step size of 0.5 Å. Defect segregation energy for a particular site α is calculated using Eq. (3)[45,46] to characterize the GB interaction with point defects,

$$E^{\alpha}_{seg} = E^{bulk}_{f} - E^{\alpha}_{f}, \tag{3}$$

where E^{bulk}_{f} and E^{α}_{f} are the defect formation energies in a perfect bulk crystal and in a crystal with a GB, respectively. A positive value of the segregation energy indicates the strong interaction of the GBs with defects.

RIS, which is a non-equilibrium process in irradiation of an alloy, usually occurs at point defect sinks beyond 200 °C.[24] In this part, the defect evolution simulation[47,48] was performed by MD simulation at different temperatures (300 K, 600 K, and 900 K). The four GB systems were conducted using the same method, consisting of about 50 000 atoms. We created randomly distributed Frenkel pairs (1 at. %) to efficiently analyze the interaction between residual defects and GBs. All systems were relaxed at the NPT ensemble for 6 ns until each system reached a stable state.

III. RESULTS AND DISCUSSION

A. Defect production near GB

1. GB type dependence on defect production

Given that the first cascade is the outset of 10 overlapped cascades and can be used to distinguish the evolution of defects, the results of the first cascade were adopted to figure out the role of GB in the defect formation or annealing stage. Figure 2(a) shows the typical time evolution of the number of point defects during the first displacement cascades. At the beginning, the number of defects in the bulk region of each system increases rapidly, reaching the peak at 0.3–0.5 ps, followed by defect recombination and GB capture defects; the number of defects then decreases. A very few defects remain as stable defect in their bulk region at approximately 63 ps. The residual number in the GB systems is less than that in the single crystal. Figures 2(b) and 2(c) show the evolution of Σ3 (112) GB. Although the reduction of defect number mainly depends on defect recombination, interstitial atoms in the GB-containing systems can also diffuse into GB and subsequently cause the decrease of residual defect number, which is different from the defect evolution of single crystals shown in Fig. S4 of the supplementary material. As shown in Fig. 2(c), four sites far from the center of the collision cascade are numbered. The vacancy labeled 1 hardly migrates at 300 K. The interstitial atom labeled 4, which locates beyond the action range of GB, did not move to the GB either. In contrast, it can be clearly seen that the interstitial atoms labeled 2 and 3 gradually migrate to the GB and eventually annihilate in the GB region.

The number of residual point defects in the bulk region vs the number of cascade overlaps in each system is shown in Fig. 3, where each data point is an averaged value of 10 independent cascades. The diagram shows that with the increase of cascade overlaps, the residual defect number in each system increases. Comparing the residual defect number in these systems with each other, the defect number in those systems with GB is significantly less than that in the single-crystal system. Furthermore, a few defects survive after relaxation in the Σ13(510) GB, while the point defect number in Σ3(111) GB is a little higher than those in other types of GB. It is obvious that different GB types have different defect absorption capabilities to the defects induced by displacement cascade.

As shown in Fig. 4(a), the number of remaining self-interstitial atom (SIA) is less than the number of vacancies in the four investigated cases, proving that the sink strength for SIAs is larger than that for vacancies at 300 K. Even if some differences exist among GBs, the MD simulation results clearly confirmed that the interstitial atoms are preferentially absorbed by the GBs and vacancies were difficult to migrate at 300 K. Thus, numerous vacancies accumulated in the matrix. Except for the defect number, the distribution of defects can be a good indicator for characterizing the influence of GB structures. The snapshots of defect distribution for the four investigated GBs when the system is stable are displayed in Fig. 4(b). The vacancies are mainly distributed in the range of about $5a_0$ from the GB in the final stable stage, whereas the distribution range of interstitials is approximately twice as far as the vacancies. Furthermore, vacancy migration energies are of the order of 0.5–1.0 eV while interstitial migration are roughly 0.01–0.3 eV in fcc metals.[49] The migration of interstitials is much faster than that of the vacancies,[50] which makes interstitials mostly move away from the core area of the cascade collision. Most of these vacancies are clustered near the GB because of the very slow migration. Meanwhile, most of the interstitials away from the GB can be absorbed by the GB because they are easier to migrate than vacancies and tend to be absorbed preferentially by GB, resulting in the existence of few SIAs. In the process of interstitials moving toward the GB, the vacancies near the GB recombine with interstitials, as shown in Fig. 2(c). However, the preferential

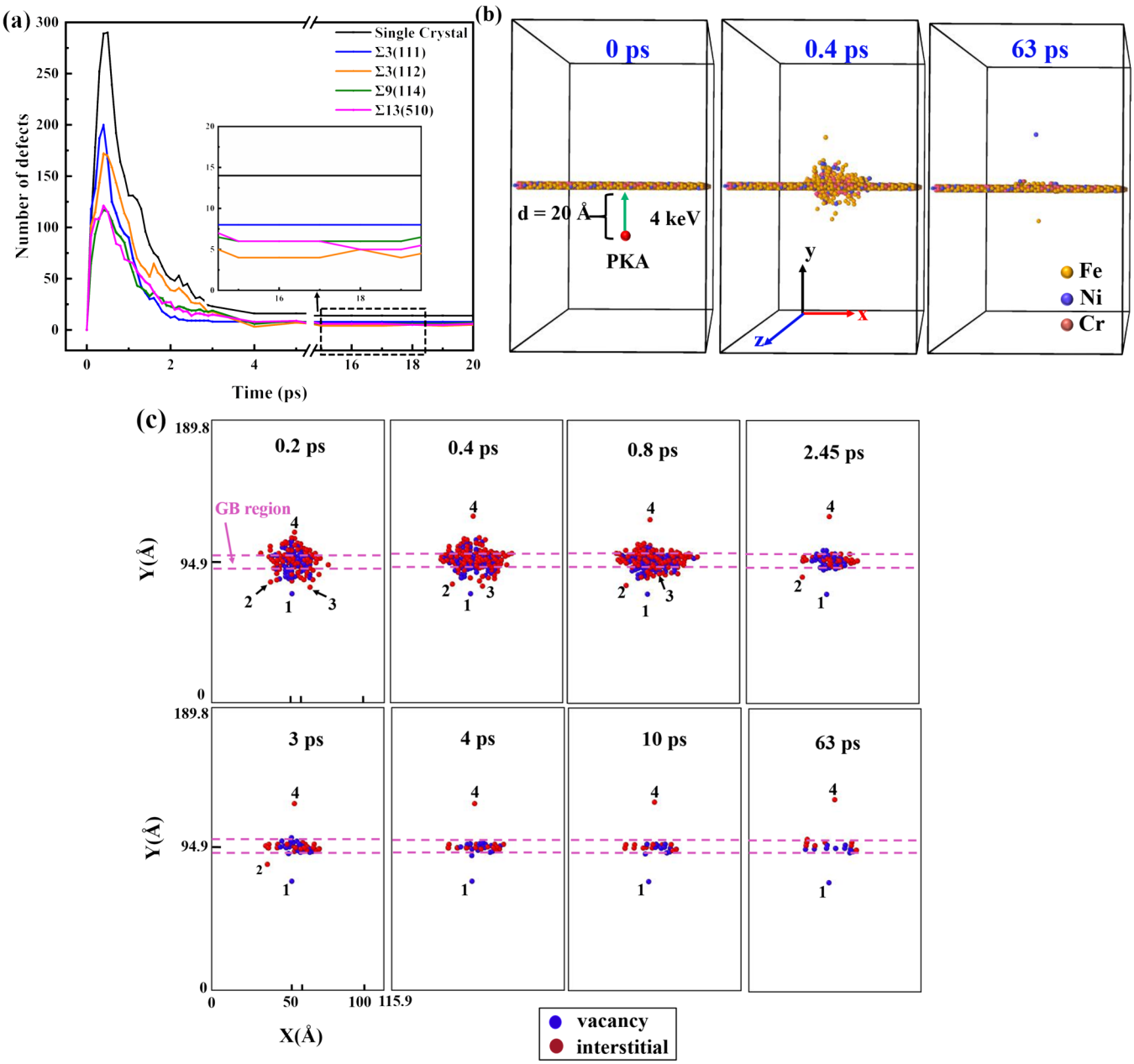

FIG. 2. (a) The time evolution of residual defects number in the bulk region of each grain boundary (GB) system and single crystal. (b) Snapshots of the displacement cascade evolution of Σ3(112) GB. (c) Snapshots of the defect structure of Σ3(112) GB. The area between the two dashed lines indicates the GB region. The four sites outside the collision cascades were marked with numbers in the picture (1: vacancy; 2–4: interstitials).

absorption of interstitial atoms also varies due to the difference in the GB structure. The number of residual interstitials is almost the same as that of vacancies in the Σ3(111) twin boundary, which is attributed to the absence of structural units and small distortion of lattice, corresponding to the relatively low GB energy. The boundary energy of Σ3(111) GB (coherent twin) is always lower than that of Σ3(112) GB (incoherent twin) and other CSL boundaries in fcc metals, as reported by studies that used experimental and theoretical approaches.[51,52] The results of boundary energy calculation of the present work in Table I are consistent with this conclusion.

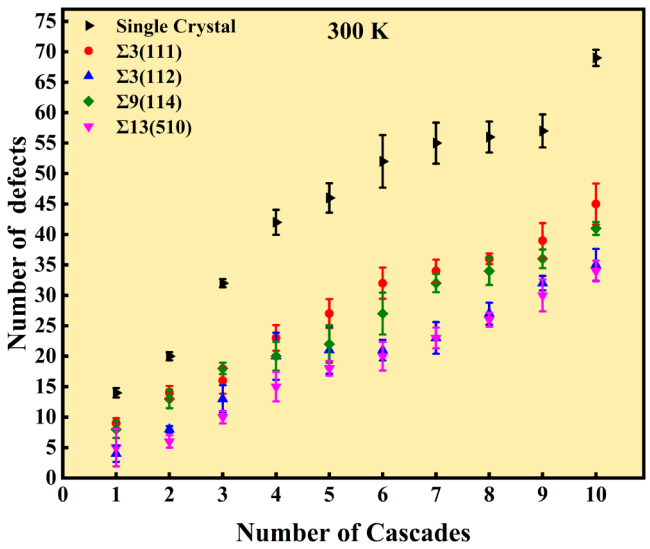

FIG. 3. Residual point defects number in the bulk region vs the number of cascades.

Furthermore, many remaining interstitials are present in the Σ9(114) GB system. The GB region is generally composed of high-pressure stress and high-tension regions, and the interstitials are inclined to be absorbed by the high-tension region.[10] Σ9(114) GB has two kinds of structural units [Fig. 1(c)]. A long-range stress field may be induced when a structural unit relaxes to a low-energy state,[53] which may weaken the preferential absorption of interstitials.

2. Energetic behavior of defects near GB

The simulation results of cumulative collision cascade indicated that the GB effectively promoted radiation-induced defect recombination and annihilation. The interstitials were more likely to migrate toward GBs than the vacancies, resulting in different spatial distributions. The formation energies of a single point defect at different distances from the GB were calculated to explore the interaction of different GB structures and defects.

In Fig. 5, the formation energy of defects (interstitials and vacancies) near each of the four GB structures was calculated as a function of distance of the defect from the GB plane. To characterize the interaction of GB with point defects, we focused on two parameters, namely, interaction width and segregation energy. "The interaction width" refers to the total distance on both sides of the

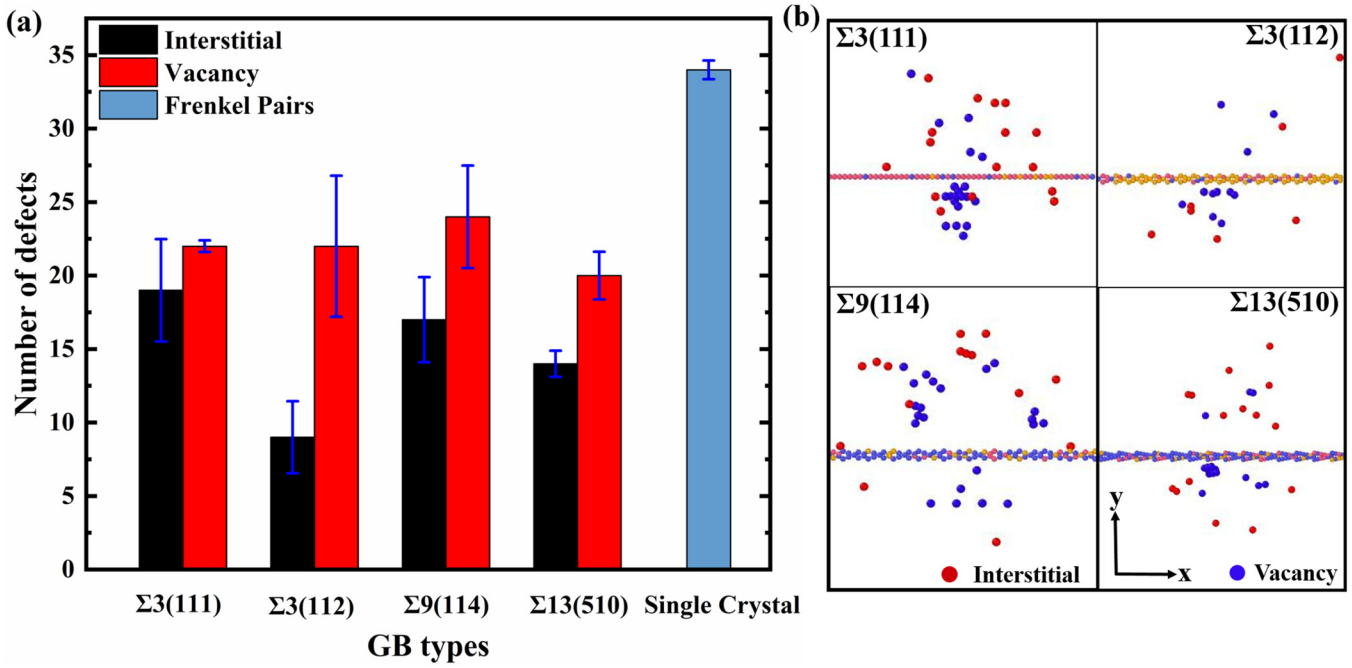

FIG. 4. (a) Number of remaining defects for all grain boundary (GB) types. For both cases, the number of remaining vacancies is higher than the remaining SIA. (b) Defect distribution at the final state for all GB types. The red and blue spheres represent interstitial atoms and vacancies, respectively. The vacancies are mostly distributed within about $5a_0$ from the GB, while the interstitial atoms are generally located beyond the range.

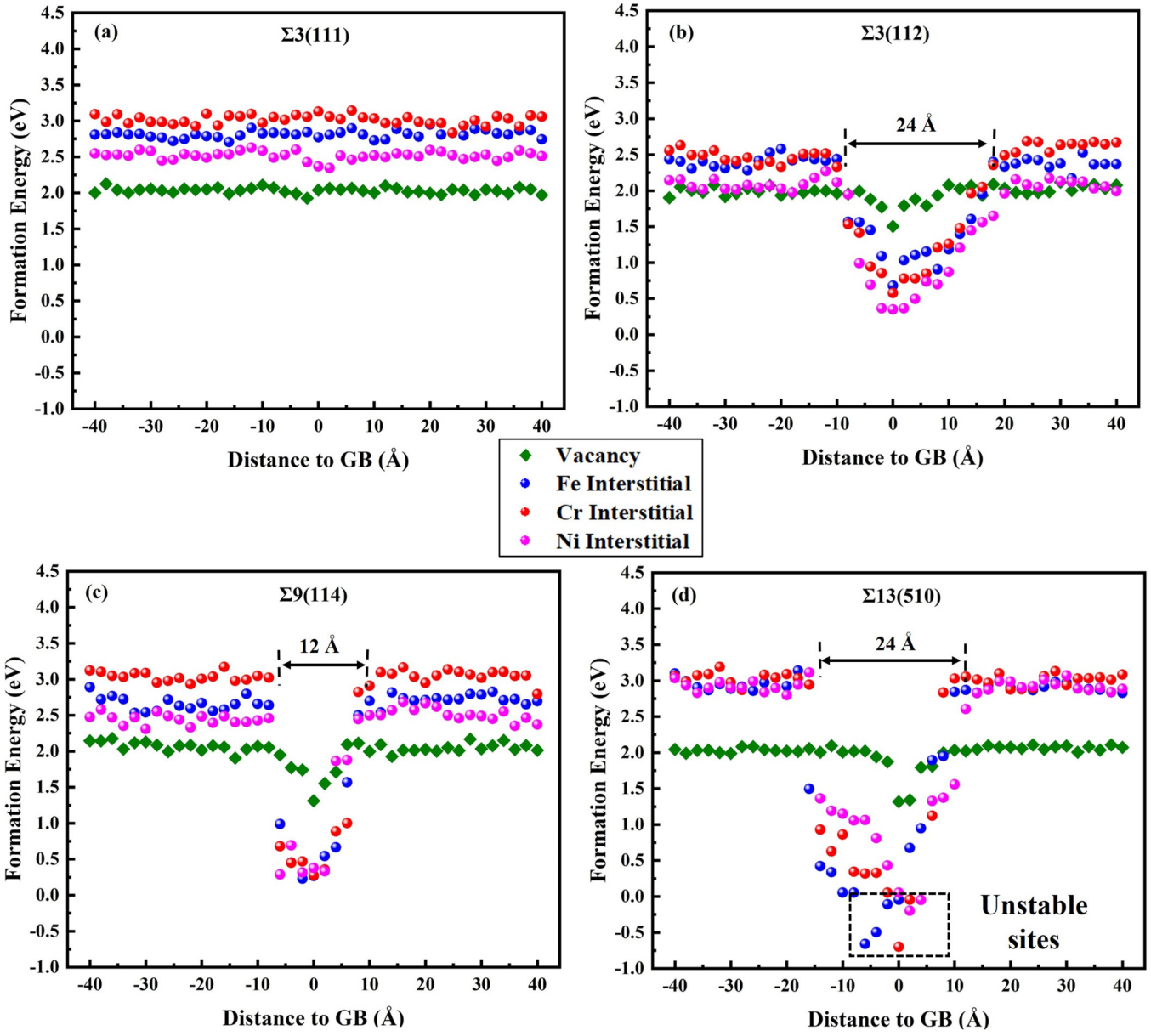

FIG. 5. Interstitial and vacancy formation energy vs distance of GB plane: (a) Σ3(111) GB, (b) Σ3(112) GB, (c) Σ9(114) GB, and (d) Σ13(510) GB. The unstable sites are marked by a black dotted box.

GB where defect energies differ by more than 10% from the bulk values. "The segregation energy" is defined by Eq. (3) mentioned in Sec. II, which refers to the difference in the formation energy of the defect in the bulk vs the formation energy in the GB. The greater the value, the stronger interaction of GBs with defects.[34,46] Table II lists the results for these four GBs.

The formation energy of defects at GB shows a downward trend compared with the matrix. As the point defect approaches the GB, its formation energy decreases. The formation energy of interstitial atoms has a considerable reduction, which means that the system energy is decreased mainly through occupying GB sites by interstitials, rather than vacancies. Except for Σ3(111) GB, the interaction strength of interstitials is stronger than vacancies in other three GBs, indicating the tendency of interstitials to form near the GB plane. In other words, interstitials are preferentially located at the GB. The formation energy can slightly vary in the

TABLE II. Segregation energy and interaction width for the four investigated grain boundary (GBs).

	Interaction width (Å)		Max. segregation energy (eV)	
GB type	Vacancy	Interstitial	Vacancy	Interstitial
Σ3(111)	0	0	0.022 842	0.075 786
Σ3(112)	8	24	0.501 76	1.951 752
Σ9(114)	8	12	0.746 248	2.763 812
Σ13(510)	8	24	0.731 22	3.718 451

bulk region of the same system due to the variation in the nearest neighboring environment of each site. The formation energy of Fe, Cr and Ni has different values in the bulk of all GB systems but is less important near the GB.

Considering the GB structures, the energetic behavior of defects near the Σ3(111) boundary is significantly different from other GB-containing systems. The interaction width of Σ3(111) GB is almost close to zero. In contrast, Σ3(112) and Σ13(510) GBs have wider interaction width corresponding to fewer residual point defects. The interstitial formation energy at some sites in the Σ13(510) GB region even reduced to a negative value. Both these factors make Σ13 (510) GB the strongest sink for the radiation induced defects.

3. Temperature effects on defect production

Under the actual condition of the reactor service, the structural materials are faced with a high-temperature environment. The role of GB at elevated temperatures is worth to explore. In this section, the influence of temperature on the GB sink efficiency for defects was investigated. When the distance from PKA atoms to the GB was also controlled to 20 Å, four temperatures of 300 K, 600 K, 900 K, and 1000 K were selected.

Figure 6(a) shows the number of defects as a function of temperature, which reflects that the number of residual defects in each system decreases with increasing temperature on the whole. The number of defects over time evolution of the Σ13(510) GB is displayed in Fig. 6(b) to clearly demonstrate the influence of temperature at various temperatures. Atomic thermal motion intensifies with increasing temperature. Thus, the time to reach peak is delayed, and the number of displaced atoms increases. The results also show that the maximum number of defects has a positive correlation with temperature, whereas the residual number of defects has a negative correlation with temperature. The number of residual defects dropped by about 25% between simulations performed for temperatures 300 K and 600 K, as well as 900 K and 1000 K, while by only 10% for temperatures 600 K and 900 K. This phenomenon is similar to the results of previous experimental study.[50] The reason is that different types of defects have different motion behavior under various temperatures. Numerous highly mobile interstitials migrate to annihilate frozen-in vacancies or form interstitial clusters at 300 K, and the motion of interstitials is intensified along with some further annihilation of frozen-in vacancies at 600 K and 900 K. But, the decreasing trend of defect number is not obvious because that the vacancies are still difficult to migrate. As shown in Fig. 6(a), the number of residual defects in the GB-containing system fluctuates little between 600 K and 900 K, especially in Σ9 (114) GB, the number of defects at 600 K is even slightly higher than that at 900 K due to the statistical errors. The interstitials in GB-containing systems are more likely to accumulate in the GB

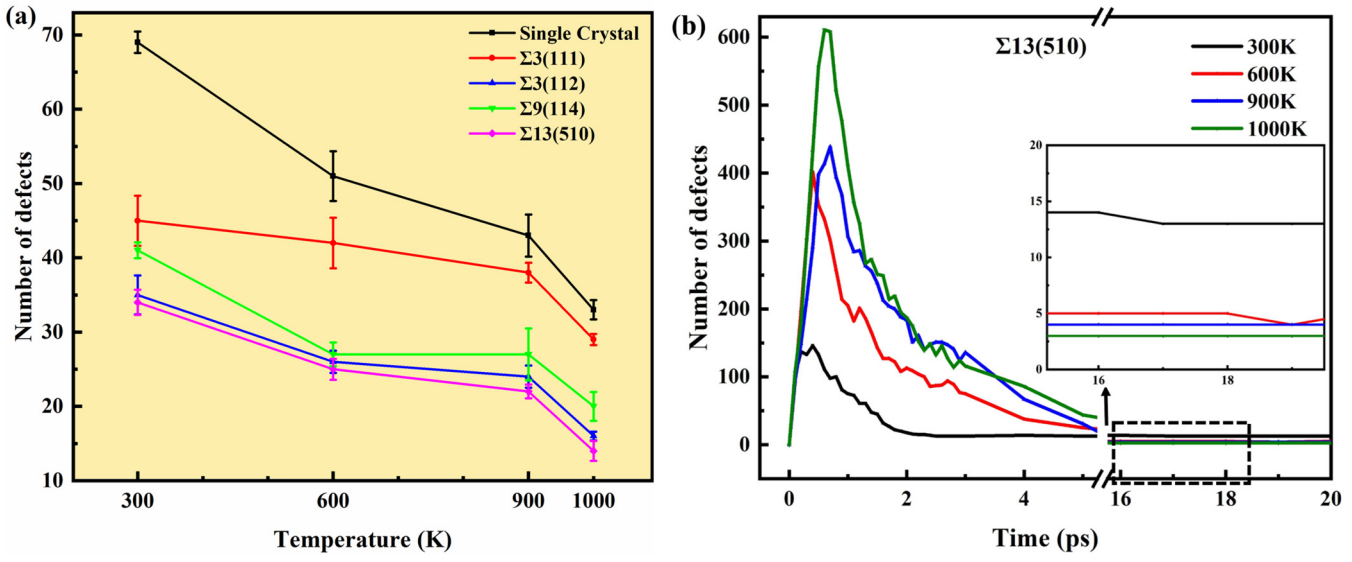

FIG. 6. (a) Number of defects in all GB-containing systems and single crystal as a function of temperature. (b) Number of defects with the simulation time in the bulk region of the Σ13(510) GB system at all temperatures.

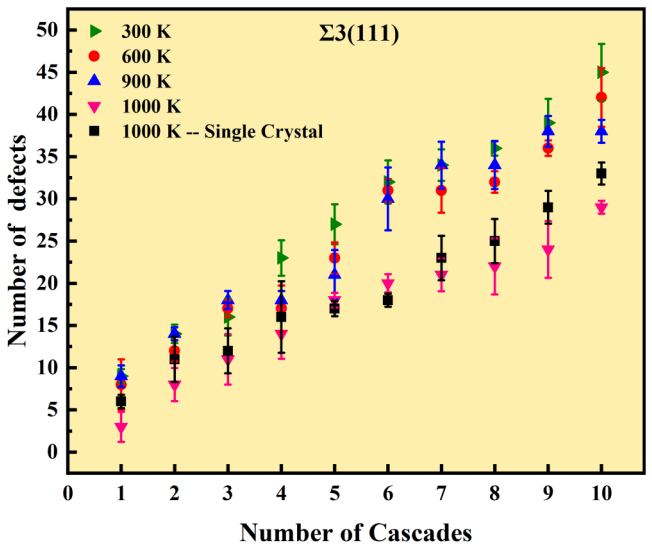

FIG. 7. Number of residual point defects in the bulk region of Σ3(111) GB vs the number of cascades at various temperatures. The number of residual defects in the single crystal at 1000 K is also shown for comparison.

region as the temperature rises, which reduces the annihilation rate of between interstitials and vacancies in the matrix so that the temperature effect on defect recombination in GB-containing systems is not significant compared to a single crystal. As the temperature increases further to 1000 K, the vacancies become mobile to annihilate interstitials, leading to a decrease in the number of defects.

In terms of the response of the GB structure to temperature, the four GB structures still function as defect sinks at various temperatures. The variation in the residual defect number with the number of cascades in the Σ3(111) GB at four temperatures is shown in Fig. 7. The residual defect number in the Σ3(111) GB system at higher temperatures till 900 K is similar to, or even more than the case at low temperature. The large-angle GBs with high energy are inclined to transform to a lower energy state by absorbing defects. Therefore, large-angle GBs are more conducive to improve the resistance of materials to radiation damage than lower energy-GBs.[54–56] The coherent twin boundaries, as a special low-energy GB, do not have superior radiation damage tolerance. These simulation results are consistent with the results in Table I. In addition, the GB energy increases with temperature and correspondingly improves sink efficiency,[57] which explains the minimum number of residual defects at elevated temperatures. From the point of view of defect formation energy, Σ3(111) GBs cannot act as effective defect sinks because their vacancy and interstitial formation energies are nearly identical to those of the bulk region [see Fig. 5(a)]. This finding also agrees with previous studies, which failed to find denuded zones in the vicinity of Σ3 twin boundaries in fcc metals, even at elevated temperatures where defect mobilities are high.[58–60] Therefore, the Σ3 coherent twin boundary is a poor sink for irradiation-induced defects compared with other boundaries. When temperature reaches 1000 K, the vacancies begin to move and recombine with the interstitials, resulting in a rapid decrease in the number of defects of each system. The defect sink effect of GBs seems not to be the main factor in defect annihilation at this temperature. Even in a single-crystal system, the number of residual defects at this temperature is small. Σ13(510) may have high GB energy due to its low GB matching. At each temperature, the number of defects in the stabilization phase is small, and the ability to absorb defects is strong.

B. Segregation near GB

RIS is directly associated with the mobile point defect flux and absorption at defect sinks, which is seriously affected by the sink efficiency of trapping point defects.[24,61–63] The ability of GB to capture defects depends on its structure, as demonstrated in Sec. III A, and temperature has a certain effect on the movement of defects near the GB. In this part, we investigated the influence of GB structure and temperature on the RIS.

Radiation-induced point defects were introduced randomly in each GB system. After the system was fully relaxed at all temperatures, the solute contents at different distances from the GB were counted. The quantitative analysis results of the relative change of chemical composition are summarized in Table III, and the data in the table present the difference in element content between the GBs and the matrix. Therefore, positive values represent the enrichment of solute elements at GBs, whereas negative values indicate depletion. As an example, Fig. 8 shows the solute concentration profiles across the Σ3(111) and Σ13(510) GBs. No visible segregation or depletion exists on the Σ3 coherent twin boundary at three temperatures, which is consistent with the experimental results of previous works.[28,64] Different degrees of Cr depletion and Ni

TABLE III. Difference between chemical composition at GB and the average value of chemical composition inside the matrix.

	The relative change of chemical composition (wt. %)								
	Ni			Cr			Fe		
GB type	300 K	600 K	900 K	300 K	600 K	900 K	300 K	600 K	900 K
Σ3(111)	−0.58	0.09	0.12	−0.11	−0.67	0.24	0.71	0.69	−0.54
Σ3(112)	0.24	0.70	1.11	−0.95	−1.49	−1.53	−0.20	−1.73	−2.94
Σ9(114)	1.40	1.75	2.12	−1.64	−2.07	−2.15	−1.88	−2.54	−4.18
Σ13(510)	2.17	2.71	3.30	−1.87	−2.73	−3.95	−2.55	−3.74	−7.68

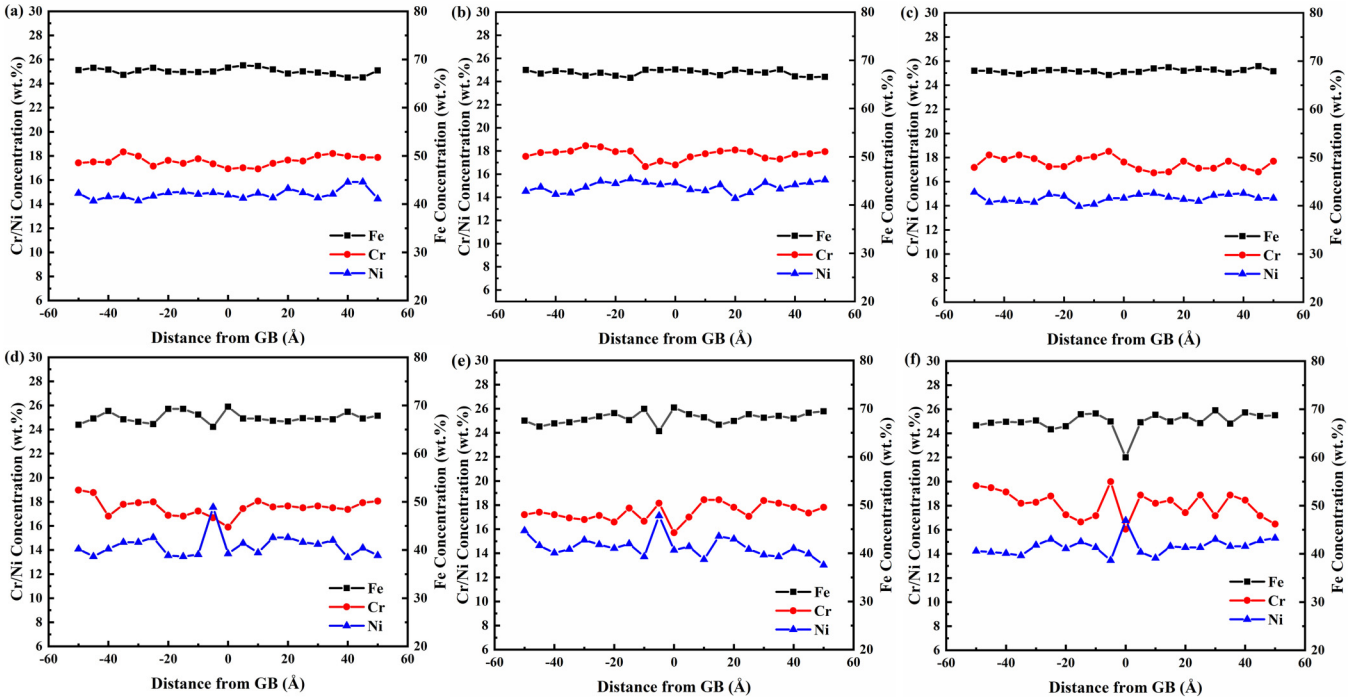

FIG. 8. Concentration profiles of Fe, Ni, and Cr in different GBs after MD simulations at T = 300, 600, 900 K: (a) Σ3(111) GB at 300 K, (b) Σ3(111) GB at 600 K, (c) Σ3 (111) GB at 900 K, (d) Σ13(510) GB at 300 K, (e) Σ13(510) GB at 600 K, and (f) Σ13(510) GB at 900 K.

enrichment occur near several other GBs, as proven by extensive experiments.[28,34,65] The phenomenon can be fully described by the inverse Kirkendall effect mechanism,[60–63] which is the preferential exchange of solute element with the vacancy flux that leads to a net flux toward or away from the boundary. The larger Cr and Fe atomic size in comparison to smaller Ni atom are favored for preferentially coupling with vacancies and subsequently depletion at GBs. The degree of segregation increased with the increase of Σ value, and similar conclusions were observed in many experiments.[26,66] This is because the higher the Σ value, the greater the degree of grain boundary mismatch, corresponding to a greater degree of lattice distortion and higher GB energy, which provides more sites for solute atoms and leads to a greater degree of segregation.[66]

In Fig. 9, the enrichment factors, which denote the ratios of the concentration in the GB over the matrix concentration,[67] is given as a function of the irradiation temperature. The enrichment

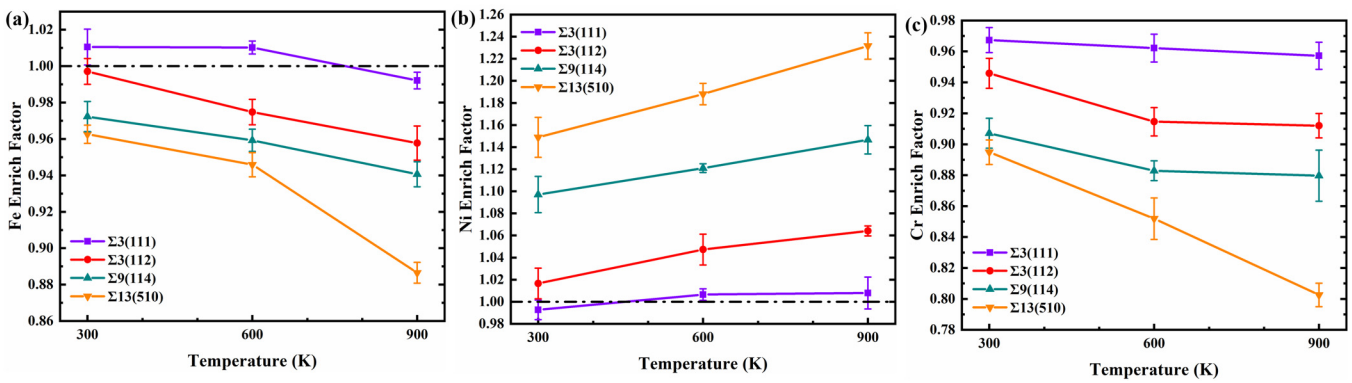

FIG. 9. Enrichment factors of each element in the four GBs as a function of the irradiation temperature: (a) Fe, (b) Ni, and (c) Cr.

factors of Fe and Cr decrease with increasing temperature, whereas the Ni enrichment factor continues to increase. Jin *et al.* found the similar trend of segregation brought by temperature in austenitic stainless steel through experimental techniques.[67] This result revealed that the degree of segregation increases with the temperature for each solute atom. In all cases of Σ3 coherent twin boundary at the three temperatures, the element content does not change and the enrichment factor of element atoms also barely changes.

Based on the inverse Kirkendall mechanism, the value of vacancy segregation energy could be an indicator of GBs to offer some information on GB structure-dependent segregation tendencies of solute atoms.[34] The Σ13 GB has the largest vacancy segregation energy among all GB structures, followed by Σ9 (Table II), and the Ni enrichment and Cr depletion on the Σ13(510) GB is remarkable. Table II shows that the vacancy segregation energies of Σ3 boundaries are relatively low, and the vacancy formation energy of coherent twin boundary is consistent with the matrix (see Fig. 5). The Σ3 GBs have lower degree of segregation than high Σ boundaries.

C. The balance between sink strength and segregation

Introducing high density of sinks is an attractive route to design radiation tolerant materials. Therefore, many researchers[68,69] have focused on the interaction between GB structure and defects to illustrate the sink efficiency. Although GBs with higher sink efficiency can capture more point defects, this does not mean that they are ideal sinks.[70] In order to evaluate the radiation effect of GBs, it is necessary to take into account its multiple effects.

It is obvious that the GB structure has great influence on both irradiation induced defects and segregation based on the present simulation results, which shows that there is a certain relationship between sink strength and RIS. Given that RIS is caused by point defect flow to a sink, the sink strength seriously affects the degree of segregation. The Σ13 and Σ9 GBs have strong sink strength because of their effective interaction with point defects, which also leads to the visible element segregation phenomenon in the vicinity of the GB in the meantime. The segregation near the Σ3(111) GB is not obvious, but the sink strength of Σ3(111) GB is weak. In addition, GBs are more capable of absorbing defects and act as efficient sinks at elevated temperatures, which is comparable with a greater degree of segregation. However, MD results show that the Σ3 non-coherent GB has strong sink strength and exhibits good resistance to solute segregation. The possible reason is that the Σ3 non-coherent GB has a larger tilt angle compared to the coherent twin boundary. It appears that the GB energy is an important factor affected by the Σ value and tilt angle, which is closely related to the segregation degree and the sink strength of GBs. Hence, by adjusting the Σ value and the tile angle of GBs, the GB energy can reach a suitable range to improve the radiation resistance of materials. Considering the sink strength and the degree of segregation of GBs, the Σ3 non-coherent GB seems to exhibit better radiation resistance.

IV. CONCLUSION

Four representative GBs in ASSs were selected to study the role of GBs in irradiation damage and the influence of GB structures on the production of defects and segregation. Simulations at different temperatures were conducted to explore the effects of temperature. Based on the main results, the following conclusions were drawn:

(1) The multiple collision cascades showed that GBs can capture the defects and promote their recombination. Thus, less defects remained in all four GB-containing systems than in a single crystal. The GBs can preferentially absorb interstitials, which leads to a higher number of vacancies remaining in the bulk region in comparison to interstitials. The MS calculations indicate that the sink strength of the GBs depends on their atomic structures. The Σ13 GB and Σ3 non-coherent boundary demonstrated strong sink strength because of their larger segregation energy and wider interaction zone, which is in agreement with the collision cascade simulations. In contrast to the non-coherent boundary, the coherent Σ3 had weak interaction with defects, matching the interaction width and segregation energy close to zero.
(2) In the simulations performed at four different temperatures (300 K, 600 K, 900 K, and 1000 K), the number of defects decreased with increasing temperature. As the temperature increases, the interaction between GBs and irradiation-induced defects intensifies. The Σ3 coherent boundary of relatively low energy has weak sink strength, and thus was less affected by temperature.
(3) Cr deletion and Ni enrichment were observed at the GBs, which was consistent with the previous experimental result. The RIS in GBs was highly dependent on the atomic structure of the GB. The Σ3 GBs could suppress deleterious Cr segregation. The Σ13 GB had the largest degree of segregation due to strong interaction with irradiation-induced defects. The degree of segregation increased with elevated temperatures.

Overall, the Σ3 non-coherent boundary showed excellent radiation resistance due to its strong sink strength and low segregation degree among the four typical GB types investigated. This type of GB can be considered in designing future ASSs of nuclear applications to improve radiation resistance.

SUPPLEMENTARY MATERIAL

See the supplementary material for the setting of PKA energy and distance, the definition of GB region, and the defect evolution of a single crystal.

ACKNOWLEDGMENTS

This work was supported by the National Natural Science Foundation of China (NNSFC) (Grant No. 11705087), the Natural Science Foundation of the Jiangsu Province (Grant No. BK20170776), and the Foundation of Graduate Innovation Center in NUAA (Grant No. kfjj20190604).

DATA AVAILABILITY

The data that support the findings of this study are available within the article and its supplementary material.

REFERENCES

[1]P. Yvon and F. Carré, J. Nucl. Mater. **385**, 217 (2009).
[2]S. J. Zinkle and G. S. Was, Acta. Mater. **61**, 735 (2013).
[3]T. Allen, J. Busby, M. Meyer, and D. Petti, Mater. Today **13**, 14 (2010).
[4]B. N. Singh, Philos. Mag. A **29**, 25 (1974).
[5]T. Liu, Q. Bai, X. Ru, S. Xia, X. Zhong, Y. Lu, and T. Shoji, Mater. Sci. Technol. **35**, 477 (2019).
[6]M. Boisson, L. Legras, E. Andrieu, and L. Laffont, Corros. Sci. **161**, 108194 (2019).
[7]X. Y. Wang, N. Gao, W. Setyawan, B. Xu, W. Liu, and Z. G. Wang, J. Nucl. Mater. **491**, 154 (2017).
[8]J. Lin, F. Chen, X. Tang, J. Liu, S. Shen, and G. Ge, Vacuum **174**, 109183 (2020).
[9]M. Samaras, P. M. Derlet, H. Van Swygenhoven, and M. Victoria, Phys. Rev. Lett. **88**, 125505 (2002).
[10]M. Samaras, P. M. Derlet, H. Van Swygenhoven, and M. Victoria, J. Nucl. Mater. **351**, 47 (2006).
[11]X. M. Bai, A. F. Voter, R. G. Hoagland, M. Nastasi, and B. P. Uberuaga, Science. **327**, 1631 (2010).
[12]M. Jin, P. Cao, and M. P. Short, Scr. Mater. **163**, 66 (2019).
[13]M. Samaras, P. M. Derlet, H. Van Swygenhoven, and M. Victoria, Phys. Rev. B **68**, 224111 (2003).
[14]E. P. Simonen and S. M. Brummer, JOM **50**, 52 (1998).
[15]C. Pokor, Y. Brechet, P. Dubuisson, J.-P. Massoud, and A. Barbu, J. Nucl. Mater. **326**, 30 (2004).
[16]S. Jublot-Leclerc, X. Li, L. Legras, M.-L. Lescoat, F. Fortuna, and A. Gentils, J. Nucl. Mater. **480**, 436 (2016).
[17]J. Malaplate, B. Michaut, A. Renault-Laborne, T. Jourdan, F. Dalle, J. Ribis, B. Radiguet, F. Sefta, and B. Décamps, J. Nucl. Mater. **517**, 201 (2019).
[18]D. J. Bacon, A. F. Calder, F. Gao, V. G. Kapinos, and S. J. Wooding, Nucl. Instrum. Methods Phys. Res. Sect. B **102**, 37 (1995).
[19]M. Samaras, P. M. Derlet, H. Van Swygenhoven, and M. Victoria, Philos. Mag. **83**, 3599 (2003).
[20]B. N. Singh and A. J. E. Foreman, Philos. Mag. **29**(4), 847 (1974).
[21]T. Toyama, Y. Nozawa, W. Van Renterghem, Y. Matsukawa, M. Hatakeyama, Y. Nagai, A. Al Mazouzi, and S. Van Dyck, J. Nucl. Mater. **425**, 71 (2012).
[22]W. Z. Han, M. J. Demkowicz, E. G. Fu, Y. Q. Wang, and A. Misra, Acta Mater. **60**, 6341 (2012).
[23]A. J. Ardell and P. Bellon, Curr. Opin. Solid State Mater. Sci. **20**, 115 (2016).
[24]G. S. Was, J. P. Wharry, B. Frisbie, B. D. Wirth, D. Morgan, J. D. Tucker, and T. R. Allen, J. Nucl. Mater. **411**, 41 (2011).
[25]S. M. Bruemmer, E. P. Simonen, P. M. Scott, P. L. Andresen, G. S. Was, and J. L. Nelson, J. Nucl. Mater. **274**, 299 (1999).
[26]T. S. Duh, J. J. Kai, F. R. Chen, and L. H. Wang, J. Nucl. Mater. **258**, 2064 (1998).
[27]J. J. Kai, F. R. Chen, and T. S. Duh, Mater. Trans. **45**, 40 (2004).
[28]S. Watanabe, Y. Takamatsu, N. Sakaguchi, and H. Takahashi, J. Nucl. Mater. **283**, 152 (2000).
[29]S. Plimpton, J. Comput. Phys. **117**, 1 (1995).
[30]P. Hirel, Comput. Phys. Commun. **197**, 212 (2015).
[31]A. Stukowski, Modell. Simul. Mater. Sci. Eng. **18**, 015012 (2010).
[32]A. V. Bakaev, D. A. Terent'ev, E. E. Zhurkin, and P. Y. Grigor'ev, J. Surf. Invest. **7**(2), 211 (2013).
[33]A. Jelea, Nucl. Instrum. Methods Phys. Res. Sect. B **425**, 50 (2018).
[34]C. M. Barr, G. A. Vetterick, K. A. Unocic, K. Hattar, X.-M. Bai, and M. L. Taheri, Acta Mater. **67**, 145 (2014).
[35]G. Bonny, N. Castin, and D. Terentyev, Modell. Simul. Mater. Sci. Eng. **21**, 085004 (2013).
[36]Y. Shibuta, S. Takamoto, and T. Suzuki, ISIJ Int. **48**, 1582 (2008).
[37]C. P. Xu, X.-Y. Liu, F. Gao, Y. H. Li, and Y. Q. Wang, Nucl. Instrum. Methods Phys. Res. Sect. B **332**, 426 (2014).
[38]H. Huang, X. Tang, F. Chen, J. Liu, and D. Chen, J. Nucl. Mater. **493**, 322 (2017).
[39]N. Swaminathan, P. J. Kamenski, D. Morgan, and I. Szlufarska, Acta Mater. **58**(8), 2843 (2010).
[40]H. Huang, X. Tang, F. Chen, Y. Yang, J. Liu, H. Li, and D. Chen, J. Nucl. Mater. **460**, 16 (2015).
[41]K. Vörtler, N. Juslin, G. Bonny, L. Malerba, and K. Nordlund, J. Phys. Condens. Matter **23**, 355007 (2011).
[42]Y. Y. Dai, L. Ao, Q. Q. Sun, J. L. Nie, S. M. Peng *et al.*, Comp. Mater. Sci. **101**, 293 (2015).
[43]J. D. Honeycutt and H. C. Andersen, J. Phys. Chem. **91**, 4950 (1987).
[44]K. Nordlund, M. Ghaly, R. S. Averback, M. Caturla, T. D. de La Rubia, and J. Tarus, Phys. Rev. B **57**, 7556 (1998).
[45]X. Li, W. Liu, Y. Xu, C. S. Liu, Q. F. Fang, B. C. Pan, J. L. Chen, G. N. Luo, and Z. Wang, Nucl. Fusion **53**, 123014 (2013).
[46]H. Huang, X. Tang, F. Chen, F. Gao, Q. Peng, L. Ji, and X. Sun, J. Alloys Compd. **765**, 253 (2018).
[47]D. S. Aidhy, C. Lu, K. Jin, H. Bei, Y. Zhang, L. Wang, and W. L. Weber, Acta Mater. **99**, 69 (2015).
[48]D. S. Aidhy, P. C. Millett, T. Desai, D. Wolf, and S. R. Phillpot, Phys. Rev. B **80**, 104107 (2009).
[49]C. C. Fu, J. Dalla Torre, F. Willaime, J. L. Bocquet, and A. Barbu, Nat. Mater. **4**, 68 (2005).
[50]R. W. Balluffi, J. Nucl. Mater. **69**, 240 (1978).
[51]G. Hasson, J.-Y. Boos, I. Herbeuval, M. Biscondi, and C. Goux, Surf. Sci. **31**, 115 (1972).
[52]J. D. Rittner and D. N. Seidman, Phys. Rev. B **54**, 6999 (1996).
[53]M. S. Laws and P. J. Goodhew, Acta Metall. Mater. **39**, 1525 (1991).
[54]K. G. Field, Y. Yang, T. R. Allen, and J. T. Busby, Acta Mater. **89**, 438 (2015).
[55]V. V. Bulatov, B. W. Reed, and M. Kumar, Acta Mater. **65**, 161 (2014).
[56]M. A. Tschopp, M. F. Horstemeyer, F. Gao, X. Sun, and M. Khaleel, Scr. Mater. **64**, 908 (2011).
[57]L. Zhang, C. Lu, K. Tieu, and Y. Shibuta, Scr. Mater. **144**, 78 (2018).
[58]M. J. Demkowicz, O. Anderoglu, X. Zhang, and A. Misra, J. Mater. Res. **26**, 1666 (2011).
[59]P. A. Thorsen, J. B. Bilde-Sørensen, and B. N. Singh, Scr. Mater. **51**, 557 (2004).
[60]P. A. Thorsen, J. B. Bilde-Sorensen, and B. N. Singh, Mater. Sci. Forum **207**, 445 (1996).
[61]H. Wiedersich, P. R. Okamoto, and N. Q. Lam, J. Nucl. Mater. **83**, 98 (1979).
[62]T. R. Allen and G. S. Was, Acta Mater. **46**, 3679 (1998).
[63]T. R. Allen, J. T. Busby, G. S. Was, and E. A. Kenik, J. Nucl. Mater. **255**, 44 (1998).
[64]N. Sakaguchi, M. Endo, S. Watanabe, H. Kinoshita, S. Yamashita, and H. Kokawa, J. Nucl. Mater. **434**, 65 (2013).
[65]K. Fukuya, M. Nakano, K. Fujii, and T. Torimaru, J. Nucl. Sci. Technol. **41**, 594 (2004).
[66]T. S. Duh, J. J. Kai, and F. R. Chen, J. Nucl. Mater. **283**, 198 (2000).
[67]H.-H. Jin, E. Ko, S. Lim, J. Kwon, and C. Shin, J. Nucl. Mater. **493**, 239 (2017).
[68]A. Esfandiarpour, S. A. H. Feghhi, and A. A. Shokri, Nucl. Instrum. Methods Phys. Res. Sect. B **362**, 1 (2015).
[69]A. Arjhangmehr, S. A. H. Feghhi, A. Esfandiyarpour, and F. Hatami, J. Mater. Sci. **51**(2), 1017 (2016).
[70]B. P. Uberuaga, S. Choudhury, and A. Caro, J. Nucl. Mater. **462**, 402 (2015).